JOURNAL OF COMPUTATIONAL PHYSICS 98, 254–268 (1992)

Orthogonal Mapping in Two Dimensions

RAMANI DURAISWAMI* AND ANDREA PROSPERETTI

Department of Mechanical Engineering, 128 Latrobe Hall, The Johns Hopkins University, Baltimore, Maryland 21218

Received October 4, 1989; revised April 24, 1991

A method for the generation of orthogonal boundary-fitted curvilinear coordinates for arbitrary simply- and doubly-connected domains is developed on the basis of the theory of quasi-conformal mappings of quadrilaterals and of previous work by Ryskin and Leal. The method has useful applications in orthogonal grid generation in two-dimensional and axi-symmetric domains and in the extension of rapid elliptic solvers and spectral methods to complex geometries. A new technique for the calculation of the conformal module of quadrilaterals is also presented.

I. INTRODUCTION

The development of mapping algorithms from an often complex "physical" domain to a simpler "computational" domain is an important subfield of contemporary research in numerical methods for partial differential equations. The literature in this area is extensive and we shall not attempt a review here. Recent reviews include those of Thompson *et al.* [1, 2], and Eiseman [3].

One of the most robust and extensively applied methods is that of Thompson *et al.* [1, 2], in which the transformed computational variables are taken to satisfy a system of Poisson equations in the original physical variables. Control on the density of the coordinate lines is obtained by adjusting the source terms of the generating equations. An alternative approach, typified by the work of Eiseman [3], is the use of algebraic interpolation methods. The mappings produced by both these methods have the disadvantage of not being, in general, orthogonal. Orthogonality endows a mapping with certain very significant advantages such as a simpler form of the transformed equations, greater ease and accuracy in the representation of boundary conditions, significantly lower discretization error, and more compact difference equations [4]. The need to extend efficient numerical techniques, such as spectral methods [5] and fast elliptic solvers [6], to more complicated geometries, requires that orthogonal mapping methods be developed.

Conformal mappings are the most well-known examples of orthogonal mappings in two dimensions. This area is one which is mathematically well understood, and various procedures for their numerical implementation may be found in the literature (see, e.g., Refs. [7–10]). For numerical purposes, the disadvantage of conformal mappings is their lack of flexibility: given a domain and its computational image, the mapping connecting them is unique if the images of any three real parameters governing the mapping are prescribed. Thus, if the images of three points on the boundary, or that of a point inside the domain and one on the boundary, are specified, the mapping is completely determined. Additionally, the inflexibility of conformal mappings causes them to be "ill conditioned" in a way that often makes them unsuitable for numerical work. As discussed, e.g., in Henrici [7], two points that are close to each other in the computational domain, can be quite far apart in the physical domain. Furthermore, a small change in the shape of the physical domain can lead to a completely different mapping.

A variant of the elliptic grid generation methods was introduced by Ryskin and Leal [12], hereafter referred to as RL, who approached the problem of orthogonality of the transformation from a covariant viewpoint. Starting from the simple observation that the physical coordinates $x_1 = x$, $x_2 = y$, trivially satisfy Laplace's equation, i.e., $\nabla^2 x_i = 0$, they carried out a transformation of variables that expresses the same equations in the computational variables ξ, η. They were thus led to the equations

$$\frac{1}{h_\xi h_\eta}\left[\frac{\partial}{\partial \xi}\left(\frac{h_\eta}{h_\xi}\frac{\partial x_i}{\partial \xi}\right)+\frac{\partial}{\partial \eta}\left(\frac{h_\xi}{h_\eta}\frac{\partial x_i}{\partial \eta}\right)\right]=0, \qquad i=1, 2,$$

where $h_\xi = [(\partial x/\partial \xi)^2 + (\partial y/\partial \xi)^2]^{1/2}$ and $h_\eta = [(\partial x/\partial \eta)^2 + (\partial y/\partial \eta)^2]^{1/2}$ are the scale factors of the transformation. The ratio

$$f(\xi, \eta) = h_\eta / h_\xi, \tag{1}$$

* Present address: Dynaflow Inc., Science Building, 7210 Pindell School Road, Laurel, MD 20707

0021-9991/92 $3.00

is termed the *distortion function*. The mapping equations of RL are then

$$\frac{\partial}{\partial \xi}\left(f\frac{\partial x_i}{\partial \xi}\right)+\frac{\partial}{\partial \eta}\left(\frac{1}{f}\frac{\partial x_i}{\partial \eta}\right)=0, \qquad i=1, 2. \tag{2}$$

Different mappings are generated by different specifications of the function f, and it is hoped that in this way some degree of control, possibly adaptive, on the distribution of coordinate lines can be achieved.

The argument that led RL to believe that the new coordinates ξ, η would be orthogonal was apparently that Eqs. (2) would take on a different form if the off-diagonal component of the metric tensor in the ξ, η space

$$g_{12}=\frac{\partial x}{\partial \xi}\frac{\partial x}{\partial \eta}+\frac{\partial y}{\partial \xi}\frac{\partial y}{\partial \eta} \tag{3}$$

were not zero, as is appropriate for orthogonal coordinates. We have found, however, that this argument is insufficient in general and that the new coordinates may not be orthogonal [13].

In addition to the question of the orthogonality of the transformed coordinates, another important point left open by the work of RL is that of the existence of the mapping and the related aspect of the latitude in the choice of the distortion function. They did not mention any constraint on f, and yet it is our experience as well as that of others [18] that, in general, f cannot be prescribed arbitrarily for an acceptable solution to exist. A simple example is the mapping of a square onto itself with the distortion function f specified to be a constant k, $k \neq 1$. Here it is easy to show that no solution with corners falling onto corners exists.

In spite of these unsolved questions that render the RL method somewhat ad hoc, several examples of its successful application can be found in the literature [14–16]. Some of the unanswered questions of the "strong constraint" method of RL were addressed in a later paper by Ascoli *et al.* [17]. However, the existence proof given there is limited to the particular case in which the conformal module of the physical domain (see Section II) vanishes. The applications given by Leal and co-workers in [14–16] do indeed fall in this category. Existence proofs for the "strong-constraint" method for more general domains, as well as for the "weak-constraint" method, are unavailable. As a matter of fact, evidence may be found in the literature of the failure of the latter algorithm for quite simple domains [18].

Building on a suggestion by Ryskin and Leal, the first purpose of the present paper is to show the connection between their formulation and the well-developed theory of quasi-conformal mappings [19, 20] explicitly. This enables us to answer some of the open questions related to their method and offers hope that all the remaining obscure aspects will be clarified completely in the near future. Such a development should give confidence in its use as a powerful computational tool in a wide variety of problems. In addition, we explicitly give a restricted class of distortion functions such that the existence of the mapping is guaranteed.

Second, we present a computationally efficient way to generate the mappings governed by Eq. (2). The class of distortion functions that we develop makes explicit use of the value of the conformal module of the physical domain. We have developed a new method to evaluate this quantity that appears to be of interest in itself and that is also described.

II. THEORY

As noted by RL, the mappings generated by Eqs. (2) can be studied in the framework of the theory of quasi-conformal mappings, of which we give a brief review. The reader interested in a more exhaustive treatment may refer to the standard texts by Ahlfors [19] and Lehto and Virtaanen [20].

II.1. *Problem Statement*

Since our goal is to construct mappings that mimic the classic orthogonal curvilinear coordinates for complicated geometries, the physical domain can be characterized as being enclosed by four continuous, non-intersecting (i.e., Jordan) arcs, whose union is a closed, non-intersecting (i.e., Jordan) curve. Such a domain, characterized by four vertices, is termed a *quadrilateral*. The vertices are denoted by P_1, P_2, P_3, and P_4, the numbering being in the positive (anti-clockwise) orientation. Doubly connected domains can also be treated in this way as, on introducing a cut, the two sides of which count as two of the four Jordan arcs, they become domains of this type. Our aim is to map this physical domain Q onto the unit square $S \equiv \{0 \leqslant \xi, \eta \leqslant 1\}$.

Throughout this paper (ξ, η) will be used to denote the coordinates in the transformed, or computational, domain, while (x, y) will be used to refer to the coordinates in the original, or physical, domain. These symbols will also be used to refer to the mapping functions connecting the two coordinate systems. The notation $\zeta = \xi + i\eta$, and $z = x + iy$, where i is the imaginary unit, is also used.

II.2. *Conformal Mapping*

Conformal mappings are the best known examples of orthogonal mappings. Although, as mentioned above, this class of mappings is too restricted for our purposes, their consideration provides a useful starting point for our discussion.

Let Q be a given physical domain of the above type. Riemann's mapping theorem states that Q can be mapped conformally to any other simply connected domain [21]. If we wish this domain to be the domain S, we cannot require

the points P_1 through P_4 to fall on the corners of the square, since the theorem implies that the mapping is completely determined when the position of three boundary points (or any other set of three real quantities) is specified [21]. However, again on the basis of the Riemann mapping theorem, it can be shown that each quadrilateral Q can be mapped conformally to a fixed class of rectangles R in such a way that the vertices of the quadrilateral, in the proper sequence, are mapped onto the corners of the rectangle [7]. This class of rectangles consists of all the rectangles that have the same *module* M, defined as the ratio of the lengths of two adjacent sides. For the purpose of conformal mappings, it is therefore seen that the module is a characteristic and fundamental property of every quadrilateral. In view of the arbitrariness in the choice of the adjacent sides, modules M and $1/M$ must be considered identical. Since the inverse of a conformal mapping is conformal, it follows that two quadrilaterals, Q_1 and Q_2, having the same module M, can be mapped onto each other conformally by using, as an intermediate step, the mapping on a rectangle with module M. In this sense, all possible quadrilaterals are divided into equivalence classes. Degenerate quadrilaterals with two coincident consecutive points (trilaterals, see, e.g., Fig. 11), or with two sets of two coincident consecutive points (lunes, see, e.g., Fig. 10), can also be put in this framework by considering them as limit cases of regular quadrilaterals, and ascribing to them modules 0 or ∞.

If the mapping from Q to R can be determined, the problem of mapping the physical region Q onto the computational region S is reduced to that of mapping R onto S. This is a particular case of the so-called Grötzsch problem, which consists of finding the mappings that transform a rectangular region R onto another rectangular region R' [19]. Historically, the theory of quasi-conformal mappings has developed from the effort to provide a solution to this problem. Before quoting this solution, it is necessary to review some elements of this theory briefly.

II.3. *Quasi-conformal Mappings*

Consider a general mapping defined in a certain region Ω of the complex plane. If the mapping transforms quadrilaterals of module M into quadrilaterals of module M', the ratio

$$D = \sup_{Q \subset \Omega} \frac{M'}{M}, \tag{4}$$

where the supremum is taken over all quadrilaterals of Ω, is termed the *dilatation* of the mapping. A mapping for which the dilatation satisfies the condition $D \leqslant K < \infty$ is termed a K-quasi-conformal mapping. The statement that a mapping is quasi-conformal in Ω implies therefore that the maximum value of the ratio of the stretchings that it induces is bounded in Ω. In other words, all mappings with finite dilatation are quasi-conformal. It is clear from this definition that conformal mappings are 1-quasi-conformal. Since modules M and $1/M$ are indistinguishable, dilatations D and $1/D$ are in principle also the same. The prevailing convention is to define the dilatation in such a way that $D \geqslant 1$, so that one need only consider the case $K \geqslant 1$. It can also be shown that a mapping and its inverse have the same dilatation.

The functional definition of quasi-conformal mappings hinges on the Beltrami equations which play a role analogous to that of the Cauchy–Riemann equations in the theory of conformal mappings. Indeed, these equations may be viewed as generalizations of the Cauchy–Riemann equations. They can be expressed in the compact form

$$\frac{\partial z}{\partial \bar{\zeta}} = \mu \frac{\partial z}{\partial \zeta}, \tag{5}$$

where $\mu(\zeta, \bar{y})$ is the *complex dilatation.* Its relation to the dilatation D defined ealier by Eq. (4) is given by

$$\sup_{\Omega} |\mu| = \frac{D-1}{D+1}.$$

From the above equation it follows that $|\mu| < 1$. For a conformal mapping, $D = 1$, $\mu = 0$, and the Beltrami equations reduce to the Cauchy–Riemann ones.

The existence theorem of quasi-conformal mappings states that, given two simply connected, conformally equivalent domains D and D' in the plane and a measurable function μ ($|\mu| < 1$), a quasi-conformal mapping between the two domains with the specified complex dilatation exists [20]. Here the provision that the domains be conformally equivalent means that it is possible to map the two domains onto each other with a mapping that is conformal everywhere and therefore rules out the possibility of mapping, e.g., the entire plane onto a bounded domain.

Upon a change of variables from $\zeta, \bar{\zeta}$ to ξ, η the Beltrami equation (5) can be expressed in terms of real variables as

$$\left(\frac{\partial x}{\partial \xi} - \frac{\partial y}{\partial \eta}\right) + i\left(\frac{\partial y}{\partial \xi} + \frac{\partial x}{\partial \eta}\right) = (\mu_r + i\mu_i)\left[\left(\frac{\partial x}{\partial \xi} + \frac{\partial y}{\partial \eta}\right) + i\left(\frac{\partial y}{\partial \xi} - \frac{\partial x}{\partial \eta}\right)\right],$$

where $\mu = \mu_r + i\mu_i$. On equating real and imaginary parts, we obtain

$$(1-\mu_r)\frac{\partial x}{\partial \xi} = (1+\mu_r)\frac{\partial y}{\partial \eta} - \mu_i\left(\frac{\partial y}{\partial \xi} - \frac{\partial x}{\partial \eta}\right), \tag{6}$$

$$(1-\mu_r)\frac{\partial y}{\partial \xi} = -(1+\mu_r)\frac{\partial x}{\partial \eta} + \mu_i\left(\frac{\partial x}{\partial \xi} + \frac{\partial y}{\partial \eta}\right). \tag{7}$$

If these relations are viewed as equations in μ_r and μ_i, it is found that, if the orthogonality condition $g_{12}=0$, with g_{12} given by (3), is to hold, $\mu_i=0$. This circumstance limits our consideration to real dilatations. We can then define a real function $f(\xi, \eta)$ such that

$$\mu_r \equiv \mu = \frac{1-f}{1+f} \tag{8}$$

In terms of this function, the Beltrami equations take the form

$$f\frac{\partial x}{\partial \xi} = \frac{\partial y}{\partial \eta}, \qquad f\frac{\partial y}{\partial \xi} = -\frac{\partial x}{\partial \eta}, \tag{9}$$

from which the connection with the Cauchy–Riemann equations, for which $f=1$, is again evident. On differentiation and elimination of x and of y, respectively, these equations reduce to the mapping equations (2) of RL.

The above argument shows that, if x and y satisfy the Beltrami equations, then they also satisfy Eq. (2) and $g_{12}=0$. However, if the coordinate generation technique is to be based on (2), a question of greater interest is the inverse one: under what conditions does satisfaction of (2) ensure orthogonality throughout Q? We have only been able to give a partial answer to this question, which is given in Section III.2 below. Further comments will be found at the end of Section V.

As already noted, the introduction of the conformally equivalent rectangle R has reduced the original problem to a particular case of the so-called Grötzsch problem, i.e., of the problem of mapping a rectangle R onto a rectangle R'. This remark has an important bearing on the question of the *existence* of the mapping. Indeed it can be shown [19] that such a mapping is K-quasi-conformal and exists if and only if the following condition is satisfied:

$$\frac{1}{K} \leqslant \frac{M'}{M} \leqslant K. \tag{10}$$

When R' is the square S, $M'=1$ and the above condition becomes

$$K \geqslant \sup(M, 1/M). \tag{11}$$

Equality is achieved in the case of the affine, or linear, mapping $\zeta = az + b$, with a and b complex constants. Any other orthogonal K-quasi-conformal transformation has $K > \sup(M, 1/M)$.

It should be noted that, although (11) ensures the existence of a quasi-conformal mapping from R to S, it does not guarantee that corners will be mapped onto corners. A simple example of this fact is the mapping between S and itself obtained by specifying the distortion function $f=K$ such that $K>1$ [13]. Hence, for our purposes, Eq. (11) is to be considered as necessary but will, in general, not be sufficient. Furthermore, as the composition of a 1-quasi-conformal mapping (i.e., a conformal mapping) and a K-quasi-conformal mapping is K-quasi-conformal, we conclude that not only the constant K of the mapping from R to S must satisfy (11), but also that the K of the total mapping must satisfy this relation as well.

In view of the relation between the distortion function f, the dilatation D, and the constant K, it is clear that Eq. (11) imposes a constraint on the class of distortion functions f that can be used to effect the mapping. Thus, while the condition $f>0$ will ensure that $|\mu|<1$, as required, it does not, by itself, ensure that the necessary condition (11) is satisfied [13], contrary to some statements in the literature [22].

A complete characterization of the class of admissible distortion functions that will map the vertices of the quadrilateral in the physical domain onto those of the unit square in the computational domain is a matter of current research. The problem is clearly very important, as it holds the key to the implementation of efficient adaptive mappings. In the following section we shall give a partial answer to this question by considering a restricted class of distortion functions.

III. A CLASS OF DISTORTION FUNCTIONS

Although we are unable to characterize admissible distortion functions in general, if the conformal module of the quadrilateral M in the physical plane is known, one can construct a simple class of mappings suitable for our purposes. This objective can be attained in the following way.

The Riemann mapping theorem guarantees the existence of a unique conformal mapping between the quadrilateral Q and a rectangle $R \equiv \{0 \leqslant \hat{\xi} \leqslant 1, 0 \leqslant \hat{\eta} \leqslant M\}$ with sides of length 1 and M. The distortion function $f = h_{\hat{\eta}}/h_{\hat{\xi}}$ for such a mapping equals unity as already noted. Now let the rectangle be mapped to an auxiliary square domain $\bar{S} \equiv \{0 \leqslant \bar{\xi}, \bar{\eta} \leqslant 1\}$, using a linear mapping that contracts or extends in the vertical direction, i.e., $\bar{\xi} = \hat{\xi}$, $\bar{\eta} = \hat{\eta}/M$. From the definition, clearly the distortion funtion for this mapping has the constant value M.

To exert further control on the mapping, we now map $\bar{S}$ onto the final computational domain S using stretching transformations acting separately on the two coordinates; i.e., we set

$$\xi = G_1(\bar{\xi}), \qquad \eta = G_2(\bar{\eta}). \tag{12}$$

To ensure that this mapping be onto and one-to-one, it is sufficient to impose that the functions G_i be strictly monotonic and that $G_i(0)=0$, $G_i(1)=1$. A similar stretching has been proposed in connection with conformal

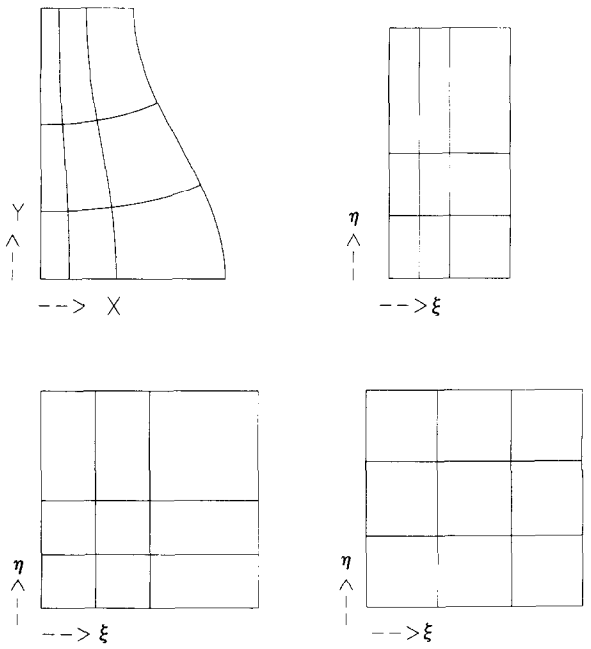

FIG. 1. Conceptual steps in the construction of the class of distortion functions (13).

mapping in Ref. [2]. The various steps used in the above construction are shown schematically in Fig. 1.

The coordinate lines resulting from the composition of the three intermediate mappings described above will be orthogonal since the first two transformations evidently preserve orthogonality and clearly the change of variables (12) does not affect the validity of the orthogonality condition, $g_{12} = 0$. Evidently, the intermediate mapping from R to $\bar{S}$ is an affine mapping for which the dilatation equals M. The final mapping is not, however, affine, and therefore the value of K for the complete mapping from Q to S will satisfy $K > M$. To compute the scale factors of the composite transformation from (x, y) to (ξ, η) it is sufficient to apply the chain rule to find

$$h_\xi = \frac{d\bar{\xi}}{d\xi} h_{\bar{\xi}}, \qquad h_\eta = M \frac{d\bar{\eta}}{d\eta} h_{\bar{\eta}}.$$

Since the first mapping from (x, y) to $(\bar{\xi}, \bar{\eta})$ is conformal, the ratio of the scale factors $h_{\bar{\eta}}/h_{\bar{\xi}}$ is unity and we find for the distortion function of the composite mapping

$$f = M \frac{d\bar{\eta}/d\eta}{d\bar{\xi}/d\xi} = M \frac{d\xi/d\bar{\xi}}{d\eta/d\bar{\eta}} = M \frac{a(\xi)}{b(\eta)}, \tag{13}$$

where

$$a(\xi) = \frac{dG_1}{d\bar{\xi}}, \qquad b(\eta) = \frac{dG_2}{d\bar{\eta}}. \tag{14}$$

It must be emphasized that the stepwise approach taken in obtaining the mapping between Q and S is only a conceptual device—in practice the mapping is done in a single step by choosing a distortion function of the type (13) at the beginning of the procedure and solving the mapping equations. In this choice it must be kept in mind that the functions a and b must be strictly positive, so that the G_i's may be monotonic, and that, for corners to be mapped onto corners, M must be the exact module of the quadrilateral. Furthermore, since $G_i(0) = 0$, $G_i(1) = 1$, from (14) we obtain the constraint

$$1 = \int_0^1 d\bar{\xi} = \int_0^1 \frac{d\xi}{a(\xi)}, \tag{15}$$

and, similarly,

$$1 = \int_0^1 \frac{d\eta}{b(\eta)}. \tag{16}$$

Finally, for the dilatation to be finite, the functions a and b cannot vanish or become infinite in the interval $[0, 1]$. It is readily verified that, because of these relations, $f \geqslant M$ at least on part of Q, so that the condition (11) be satisfied.

The preceding argument has enabled us to construct a broad class of distortion functions that are guaranteed to result in orthogonal mappings. These functions enable one to have some control over the density of the coordinate lines by varying the stretching determined by a and b which, from the above analysis, are seen to have a clear meaning. Locally, large values of a will give a large density of lines $\xi = \text{const}$, while large values of b will produce a fine distribution of lines $\eta = \text{const}$. A particularly valuable feature of the preceding class of distortion functions is that substituting them into the mapping equations (2) gives rise to separable equations. As will be seen below, this feature permits an efficient numerical solution of the equations and of certain physical problems posed on such domains.

This approach to the construction of orthogonal mappings is not new and can be found elsewhere, e.g., in Ref. [22], where, however, the restrictions previously given on the functions a and b are not made explicit.

III.1. *More General Distortion Functions*

Orthogonal mappings with distortion functions having a form different from that developed before are of course possible and, in fact, highly desirable to achieve a more localized control on the density of coordinate lines. The previous developments may point the way to a proper definition of this problem.

Let L_i be the length of the side of the quadrilateral Q

between the vertices P_i and P_{i+1} (with $P_5 \equiv P_1$). With the convention shown in Fig. 1, the side L_1 is mapped onto $\xi = 1$, L_2 onto $\eta = 1$, L_3 onto $\xi = 0$, and L_4 onto $\eta = 0$. From the geometric significance of the scale factors it is obvious that the integral conditions

$$\int_0^1 h_\xi|_{\eta=0,1}\, d\xi = L_{4,2}, \qquad \int_0^1 h_\eta|_{\xi=0,1}\, d\eta = L_{3,1}$$

must be satisfied, since only in this case will corners fall onto corners. Equations (15) and (16) are a consequence of these relations and of the existence of a conformal mapping of Q onto the conformal rectangle R. Furthermore, to ensure that (11) is satisfied, so that the mapping is quasi-conformal, f must exceed M somewhere in S. This condition will ensure that the mapping does not have folds in the domain.

It may be conjectured that these conditions are necessary and sufficient for the existence of the required orthogonal mappings. That this is indeed the case, of course, still awaits a proof. In any case, even if the conjecture can be proven, a way must be found to efficiently enforce these constraints in the construction (possibly adaptive) of general distortion functions.

III.2. *Degenerate Quadrilaterals*

As mentioned above, degenerate quadrilaterals are those for which one or two non-adjacent sides degenerate to points. Since in this case a point in the physical space is mapped to one side of the computational square, the maximum dilatation is not finite and the resulting mapping not quasi-conformal. However, in some cases, one can dispense with the theory of such mappings, because the Riemann mapping theorem can be used directly.

Let us address the case of a lune-shaped region first, because it is simpler. The Riemann mapping theorem guarantees the existence of a conformal mapping such that the lune is mapped onto the unit circle in the $(\tilde{\xi}, \tilde{\eta})$ plane with its two vertices mapped on $\tilde{\xi} = \pm 1$, $\tilde{\eta} = 0$. The further transformation

$$\exp(\hat{\xi} + i\hat{\eta}) = \frac{\tilde{\xi} - i\tilde{\eta} + 1}{\tilde{\xi} - i\tilde{\eta} - 1},$$

which is conformal, maps the circle onto the infinite strip $-\infty < \hat{\xi} < \infty$, $\frac{1}{2}\pi \leqslant \hat{\eta} \leqslant \frac{3}{2}\pi$. Finally, the orthogonal transformation

$$\bar{\xi} = \frac{1}{1 + \exp(-\hat{\xi})}, \qquad \bar{\eta} = \frac{1}{\pi}\hat{\eta} - \frac{1}{2},$$

maps the infinite strip onto the square $0 \leqslant \bar{\xi}, \bar{\eta} \leqslant 1$. At this point, the stretching argument previously used can be applied, introducing functions a and b subject to the same restrictions as before. Since the ratio of scale factors for the conformal transformations of this sequence is 1, the appropriate form of the distortion function is readily calculated to be

$$f = \pi\bar{\xi}(1 - \bar{\xi})\frac{a(\xi)}{b(\eta)}. \tag{17}$$

Note that, unlike the previous cases, f cannot be expressed directly in terms of ξ and η without the explicit knowledge of the function G_1 defined in (11).

For trilaterals, let us consider first the case in which two consecutive sides are straight with equal lengths, while the third side is arbitrary. Let P_1 be the vertex where the two straight sides meet and let P_2 and P_3 denote the other two vertices. Further, let α be the (interior) angle at P_1. The stretching coordinate transformation $\hat{r} = r$, $\hat{\theta} = 2\pi\theta/\alpha$ maps the physical domain onto a circle-like domain in which the two straight sides appear as the two sides of a cut running between P_1 and the two coincident images of P_2 and P_3. The Riemann mapping theorem guarantees that this domain can be mapped onto the unit circle in such a way that the point P_1 is mapped onto the center of the circle and the point(s) P_2, P_3 is mapped onto the point $\bar{r} = 1$, $\bar{\theta} = 0$. Polar coordinates stretched by 2π now map this circle onto the unit square $0 \leqslant \bar{\xi}, \bar{\eta} \leqslant 1$, and a further stretching transformation can be carried out as before. The final distortion function for the composite mapping is easily seen to be given by

$$f = \alpha\bar{\xi}\frac{a(\xi)}{b(\eta)}. \tag{18}$$

As before, the function G_1 must be known to express this result in terms solely of ξ, η. This is similar to the construction used by Ascoli *et al.* [17] in their proof of the validity of the RL mapping procedure for a simply connected physical domain when it is desired to map the entire boundary onto one side of the computational domain.

The previous procedure evidently fails for more general trilaterals. The generation of suitable orthogonal mappings in this case is a question that must be left open at the present time. In particular, this comment applies to some of the domains considered in Ref. [12] for which $\alpha = \pi$, but the two straight sides are not necessarily of equal length.

Since in the physical plane the degenerate points are concentration points for the coordinate lines, the corresponding scale factors must vanish at these points. From the definition (1) of f it is therefore seen that, in these cases, f must vanish when the degenerate point is mapped to a line of constant ξ as in the procedures described above. The explicit forms (17) and (18) of the distortion functions given above

satisfy this restriction. If the degenerate point(s) were mapped to a line of constant η, the function f would become infinite there. As the construction of the distortion function for these degenerate cases does not need knowledge of the conformal module, such domains can be mapped with less computational effort than the quadrilaterals considered previously. Examples of the orthogonal mapping of degenerate quadrilateral domains will be given in Section VI.

III.3. *Orthogonality*

A question of the utmost importance that we have not yet addressed is that of the boundary conditions under which the mapping equations (2) should be solved. Since, in these equations, the two coordinates are uncoupled, it is obvious that any mutual relationship between the coordinate lines, such as orthogonality, must arise from the imposition of suitable boundary conditions. Here we prove that, at least for the class of distortion functions considered here, the imposition of the condition $g_{12}=0$ along the boundary results in orthogonal coordinate lines throughout the domain. The first step is to verify by direct substitution that

$$\hat{g}_{12}=\frac{\partial x}{\partial \hat{\xi}}\frac{\partial x}{\partial \hat{\eta}}+\frac{\partial y}{\partial \hat{\xi}}\frac{\partial y}{\partial \hat{\eta}}$$

satisfies Laplace's equation in the $\hat{\xi}, \hat{\eta}$ coordinates. Therefore, if this quantity vanishes on the boundary, by a well-known theorem, it also vanishes inside the domain. Next, we express g_{12} in terms of $\hat{g}_{12}$ by the chain rule to find

$$g_{12}=\frac{M}{ab}\hat{g}_{12}.$$

Since M/ab is everywhere strictly positive and finite, the vanishing of $\hat{g}_{12}$ ensures the vanishing of g_{12} as well so that the coordinate lines are indeed orthogonal inside the domain as required.

Some comments on the general case, where the distortion function is not constrained to have the form (13), are contained in Section V.

IV. CALCULATION OF THE CONFORMAL MODULE

The use of distortion functions of the class defined above requires the explicit knowledge of the conformal module of the physical domain. As already noted, this quantity is an intrinsic property of any quadrilateral domain and is a fixed number once the boundary arcs of the quadrilateral have been chosen. A discussion of earlier methods used to calculate the conformal module may be found in Gaier [23, 24]. A basic theorem (that extends to degenerate quadrilaterals as well) states that, given a sequence of quadrilaterals Q_n that tend to a quadrilateral Q, then

$$\lim_{n\to\infty} M(Q_n)=M(Q).$$

This result allows one to estimate the module by approximating the given domain and calculating the module of the approximate domains.

The methods of evaluating the module can be broadly divided into two classes. One class relies on the fact that, given a conformal mapping between the domain of interest and a rectangle, the module is simply the ratio of the adjacent sides of the rectangle. These methods are evidently only useful in special cases where the form of the mapping is known a priori, such as domains to which the Schwarz–Christoffel transformation can be applied. An example of methods of this type has been given by Trefethen [25], who uses it for the calculation of the module of polygonal domains. For such cases the module is calculated extremely accurately. However, this method cannot efficiently be extended to general domains by considering them as limiting cases of polygonal ones, as the necessary computational work increases proportionally to the cube of the number of sides of the polygon.

The second class of methods is based on the following characterization of the module (see, e.g., Ref. [7]). Consider, in the quadrilateral domain Q, the solution ϕ to the problem

$$\nabla^2\phi=0 \tag{19}$$

$$\begin{aligned}&\phi=1 \quad \text{on } \Gamma_1, \qquad \phi=0 \quad \text{on } \Gamma_3,\\ &\frac{\partial\phi}{\partial n}=0 \quad \text{on } \Gamma_2, \Gamma_4,\end{aligned} \tag{20}$$

where $\Gamma_1+\Gamma_2+\Gamma_3+\Gamma_4=\Gamma$ is the boundary of Q, and the numbering is in the positive orientation. The module is then given by

$$M=\int_{\Gamma_1}\frac{\partial\phi}{\partial n}\,ds, \tag{21}$$

where s denotes the arc length along Γ_1. Several methods are based on the solution, by finite differences or finite elements, of this problem [23, 24]. Our starting point is also this formulation, but we effect the calculation through the boundary element method. This approach is attractive, as the previous formulation shows that the evaluation of the module does not require the knowledge of ϕ inside Q, but only of $\partial\phi/\partial n$ on the boundary of Q, and this is exactly the quantity given by the boundary element calculation.

Application of Green's identity to the problem yields the

following integral relation satisfied by the value of ϕ at the generic point $\mathbf{x}$ of the boundary Γ,

$$c\phi(\mathbf{x}) = \int_\Gamma G(\mathbf{x}, \mathbf{x}') \frac{\partial}{\partial n_{\mathbf{x}'}} \phi(\mathbf{x}')\, ds_{\mathbf{x}'} - \int_\Gamma \phi(\mathbf{x}') \frac{\partial}{\partial n_{\mathbf{x}'}} G(\mathbf{x}, \mathbf{x}')\, ds_{\mathbf{x}'}, \tag{22}$$

where $G = \log|\mathbf{x} - \mathbf{x}'|$ is the free-space, two-dimensional Green's function. The constant c equals the aperture of the angle under which the domain is seen from the point $\mathbf{x}$. If $\mathbf{x}$ is such that a unique normal to the boundary can be defined there, the value of c is π.

Subdividing Γ into N arcs, and introducing a local coordinate σ^j which, without loss of generality, may be assumed to vary over the range (0, 1) in each subdivision, we obtain

$$c\phi(\sigma^i) = \sum_{j=1}^{N} \left\{ \int_0^1 \psi(\sigma^j)\, G(\mathbf{x}(\sigma^i), \mathbf{x}'(\sigma^j))\, J(\sigma^j)\, d\sigma^j \right.$$

Here we have set $\psi = \partial\phi/\partial n$, and J is the Jacobian of the transformation from the arc length to the variable σ, which we take to be the normalized chord length between successive nodes. The simple boundary conditions (20) for the potential problem considerably simplify the discretized form of the integral equation. Further simplification can be achieved by observing that it is necessary to solve the problem only so far as to be able to evaluate the integral in the expression (21) for the module.

The above equation may now be approximated by introducing a suitable set of local basis functions and by using these to approximate both the geometry and the unknowns ϕ and ψ. After performing the discretization, we perform the integrations in (23) and solve the resulting system by collocation. Two implementations of the above algorithm have been developed. One version uses linear basis func-

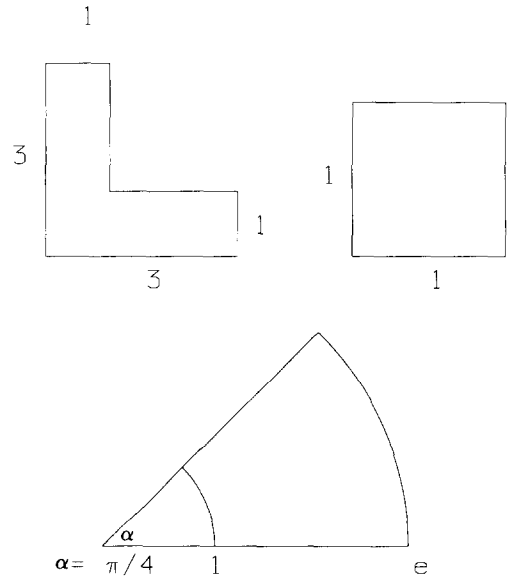

FIG. 2. Domains for which the present algorithm for the calculation of the conformal module has been tested. See Section IV and Table I for details.

TABLE I

Comparison Between the Exact Values of the Module for the Domains of Fig. 2 and the Numerical Results Given by the Method of Section IV

Fig. 2	Calculated M	Exact M
a	4.55815	4.55873
b	1.00009	1.00000
c	1.27321	1.27324

tions, in which domains with boundaries with large curvature are encountered, use was made of a second code in which ϕ and ψ are approximated linearly, while cubic splines are used for the geometry. This code uses Gaussian quadrature to do the integration.

The method was tested against one problem also solved with Trefethen's code SCPACK [26], which yields "exact" results (Fig. 2a), and also against two analytical results (Figs. 2b and c). The computations were carried out in double precision. A comparison is presented in Table I.

V. THE MAPPING ALGORITHM

Once the conformal module of the given domain has been determined and a suitable distortion function constructed, the mathematical formulation of the present mapping problem is given by

$$\frac{\partial}{\partial\xi}\left(f\frac{\partial x}{\partial\xi}\right) + \frac{\partial}{\partial\eta}\left(\frac{1}{f}\frac{\partial x}{\partial\eta}\right) = 0, \tag{24}$$

$$\frac{\partial}{\partial\xi}\left(f\frac{\partial y}{\partial\xi}\right) + \frac{\partial}{\partial\eta}\left(\frac{1}{f}\frac{\partial y}{\partial\eta}\right) = 0, \tag{25}$$

to be solved in S: $(0 \leqslant \xi, \eta \leqslant 1)$, subject to the boundary conditions

$$\frac{\partial x}{\partial\xi}\frac{\partial x}{\partial\eta} + \frac{\partial y}{\partial\xi}\frac{\partial y}{\partial\eta} = 0, \tag{26}$$

along the four arcs

$$F_i(x, y) = 0, \qquad i = 1, ..., 4. \tag{27}$$

The discretized solution of this problem will consist of a series of lines in the physical (x, y) plane corresponding to constant values of the transformed coordinates ξ, η.

Equations (24) and (25) are elliptic for $f > 0$ and, while they are linear, they are coupled through the boundary conditions (26) and (27). The nonlinear nature of these boundary conditions constitutes the major challenge to the solution of the mapping problem. We describe here a finite-difference method. A spectral method is currently under development.

Since we restrict ourselves to distortion functions of the form (13), the mapping equations are separable and Swarztrauber's finite-difference technique for the solution of elliptic separable equations [6] can be applied. For standard boundary conditions, this method yield the direct solution of such problems in the time taken for about four or five SOR iterations. A subroutine, from the package FISHPAK [27], developed for the implementation of this technique was used in our calculations.

The boundary conditions (26) and (27) must be imposed in a way that allows the use of the above subroutine, in the sense that only the solution of standard Dirichlet or Neumann boundary-value problems is required. This is done iteratively as follows. For the purpose of illustration consider the $\xi = 1$ boundary, along which η varies from 0 to 1 (Fig. 3). Let the equation of this curve be

$$F(x(\xi = 1, \eta), y(\xi = 1, \eta)) = 0.$$

Differentiating, on $\xi = 1$ we can then write

$$\frac{\partial F}{\partial x}\frac{\partial x}{\partial \eta} + \frac{\partial F}{\partial y}\frac{\partial y}{\partial \eta} = 0. \tag{28}$$

On substituting from (28) in the orthogonality condition (26) and re-arranging of terms, we have

$$\left(\frac{\partial F}{\partial y}\frac{\partial x}{\partial \xi} - \frac{\partial F}{\partial x}\frac{\partial y}{\partial \xi}\right)\frac{\partial x}{\partial \eta} = 0,$$

from which we deduce that the following equivalent boundary conditions may be imposed:

$$\left(\frac{\partial F}{\partial y}\frac{\partial x}{\partial \xi} - \frac{\partial F}{\partial x}\frac{\partial y}{\partial \xi}\right) = 0, \tag{29}$$

$$F(x, y) = 0. \tag{30}$$

It can be shown that the above equations hold even for the case $\partial x/\partial \eta = 0$.

Suppose that an estimate of the positions $\{P_j\}$, where the coordinate lines meet the boundary line $\xi = 1$, is known. These are used as Dirichlet boundary conditions and the solution to the field equations (24) and (25) is obtained. This solution will consist of an estimate of the image of the lines $\xi = \text{const}$ and $\eta = \text{const}$ in the physical plane. Consider now, for example, a line $\eta = \hat{\eta} = \text{const}$ (see Fig. 3), meeting the boundary $\xi = 1$ at a point P_j. We retain the interior points and estimate a new position P_* for this point as follows. The ξ derivatives are approximated using one-sided (backward in this case) fourth-order differences, based on the computed values of (x, y) corresponding to the interior points $\xi_I, \xi_{I-1}, \xi_{I-2}$, and ξ_{I-3}, along the line $\eta = \eta_j$. Here the notation is such that $x_i^j = x(\xi_i, \eta_j)$ and the total number of nodes in the ξ direction is $I + 1$. In this way one obtains a system of the type

$$\left(\frac{25}{12}x_{I+1}^j - A\right)\frac{\partial F}{\partial y} - \left(\frac{25}{12}y_{I+1}^j - B\right)\frac{\partial F}{\partial x} = 0, \tag{31}$$

$$F(x_{I+1}^j, y_{I+1}^j) = 0, \tag{32}$$

where

$$A = -4x_I^j + 3x_{I-1}^j - \tfrac{16}{12} + \tfrac{1}{4}x_{I-2}^j,$$

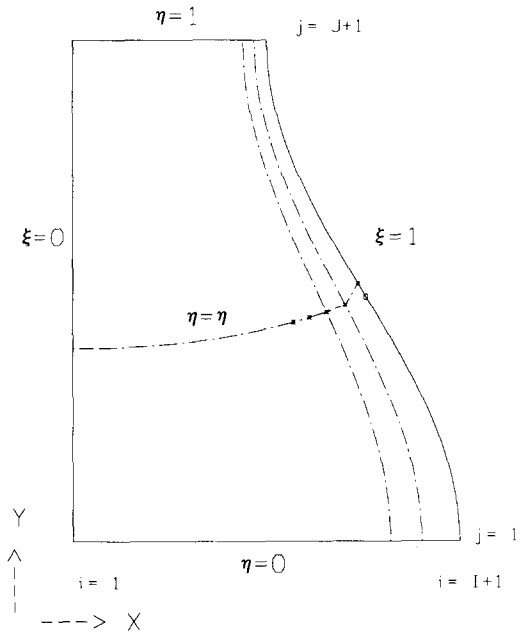

FIG. 3. Details of the boundary algorithm. The figure shows, in the physical space, the $\xi = 1$ boundary, along which η varies from 0 to 1. The dashed lines inside the domain show the coordinate lines $\xi = \text{const}$ and $\eta = \text{const}$ at the current iteration. New positions for the boundary points are generated using the orthogonality condition. The starred points, along $\eta = \hat{\eta}$, are used in the finite-difference approximation of the derivatives in the ξ direction. The circled point represents the new position of the boundary point.

and B is obtained from A by changing x into y. This system is solved by using the Newton–Raphson technique to obtain new values for the boundary coordinate x_*, y_*. A similar procedure is followed for each boundary point. The updated values x_* and y_* for each node are then used as Dirichlet boundary conditions for the field equations, and the process is repeated until the displacements $|x_* - x^j_{I+1}|$, $|y_* - y^j_{I+1}|$ of all the boundary points are below a certain tolerance. Since Eqs. (30) and (31) are part of an iterative procedure, it is not necessary to solve them to a high degree of accuracy. The computations at each node along the boundary are independent of each other so that full advantage can be taken of parallel computer architectures and also of vectorization.

A straightforward variant of this procedure can be used when the boundary is given by points instead of equations, or where the evaluation of the Jacobian required by the Newton–Raphson method is expensive. Splines are fitted through a distribution of points on the boundary, and the calculations are performed in terms of the spline parameter t. Thus, if the boundary lines are given by $x = X(t)$ and $y = Y(t)$, Eq. (25) can be written as

$$\frac{\partial X}{\partial t}\frac{\partial x}{\partial \xi} + \frac{\partial Y}{\partial t}\frac{\partial y}{\partial \xi} = 0. \tag{33}$$

The ξ-direction derivatives are approximated using finite differences, which lead to relations of the form

$$\left[\frac{25}{12}x(t_j) - A\right]\left.\frac{\partial X}{\partial t}\right|_{t_j} + \left[\frac{25}{12}y(t_j) - B\right]\left.\frac{\partial Y}{\partial t}\right|_{t_j} = 0, \tag{34}$$

with A and B as before. At each point, this equation is solved for the new variable t_* by using the Newton–Raphson technique. The values $X(t_*)$ and $Y(t_*)$ are then used as Dirichlet boundary conditions for the field equations and so forth as before.

A significant simplification of the previous procedure occurs when some of the boundary arcs of the domain are straight and parallel to the x or y axes. Here the corresponding boundary condition becomes a simple Neumann condition for one of the variables and a simple Dirichlet condition for the other. Iterations on such boundaries are not needed.

The above boundary iteration is nested inside an outer iteration where Eqs. (24) and (25) are solved using the fast solver. We have found that the first boundary iteration results in a much greater displacement of boundary points than subsequent ones. Therefore, we have used only one boundary iteration for each outer iteration. Convergence of the scheme has been tested by providing different initial guesses to the boundary point distribution and checking that the solutions obtained were the same.

As a concluding comment we return to the question of the appropriate conditions that would ensure orthogonality throughout the domain in the case of general distortion functions. Whatever the distortion function, it is evident that satisfaction of the boundary orthogonality relation (26) is a necessary condition on the mapping. Provided it converges, for any f, the algorithm just described leads to a well-defined solution of the problem posed which cannot be subjected to any further constraint. This remark strongly suggests that boundary orthogonality is also a *sufficient* condition for the mapping, so that solution of the problem (24) to (27) would lead to an orthogonal mapping in every case, provided of course that f is suitably chosen. Two difficulties, however, can arise. The procedure may not converge, or the final solution may fail to be orthogonal inside the domain. The first possibility hinges on the question of the existence of the mapping. If a suitable f is chosen, such that (10) holds, and the mapping exists, then, by continuity, there must be a non-empty set of initial guesses for the distribution of boundary points such that the orthogonal mapping is found. The boundary orthogonality condition would then also be sufficient to ensure orthogonality throughout the domain. The second possibility hinges instead on the uniqueness of the solution to the non-linear boundary-value problem posed by Eqs. (24) to (27). If more than one solution exists, it may happen that some solutions correspond to orthogonal mappings while others do not. This possibility must be left open at the present time. However, it can be stated that, at least for some initial guesses, the previous algorithm will *always* lead to an orthogonal mapping for suitable distortion functions.

VI. APPLICATIONS

We now consider some examples chosen to give a stringent test of the method and of the algorithm described in the preceding sections. All the calculations to be described have been carried out in single precision on a VAX station 3200. The grid used was 33×33, with fourth-order accurate finite-difference schemes. Between 30 and 40 iterations were completed per minute of CPU time, a figure that includes a substantial overhead for the calculation of auxiliary quantities that would not normally be required in applications. To avoid biasing the results in any way, in all cases the iterative procedure was started with an equispaced distribution of points along the boundaries. In several applications, e.g., a boundary evolving in time, an initial guess quite close to the final solution may be available. The iterations were stopped when the greatest displacement of the boundary points was smaller than 10^{-4}. Since in the following applications the linear size of the domains is of order one, there was no need to scale this number. Our experience is that, loosening the convergence criterion to 10^{-3} reduces the number of iterations by a factor of two. Although we have not systematically

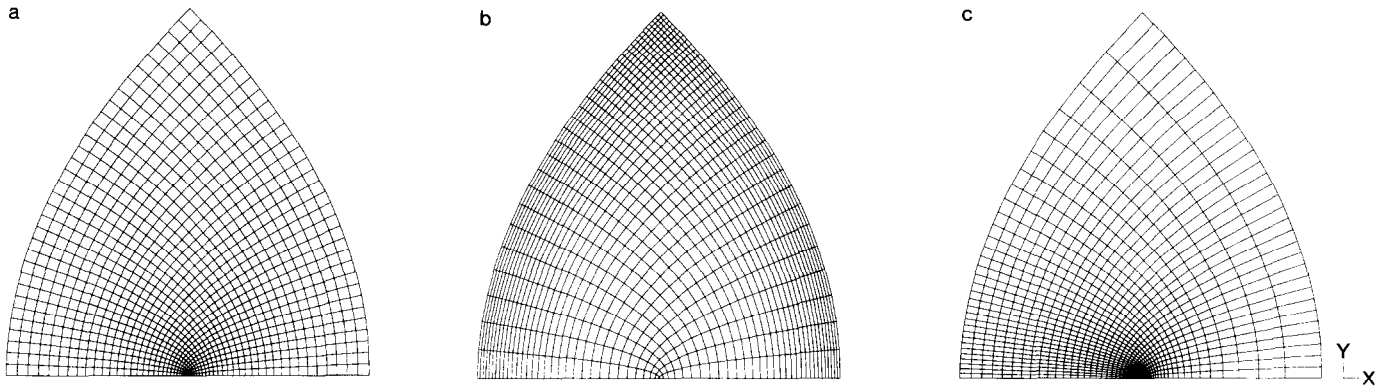

FIG. 4. Lines of constant ξ and η in the physical domain for several mappings of the region defined by $z=\zeta^2$ for $0\leqslant\xi,\eta\leqslant 1$. Figure 4a is for the conformal mapping obtained with $f-1$. Figures 4b and c show the mappings obtained with the distortion functions given in the text.

explored the matter, we have found that convergence can be accelerated by nearly an order of magnitude by use of point-SOR techniques.

The criterion used to terminate the iterations does not refer directly to the orthogonality of the mesh. When convergence has been achieved, to check orthogonality, for each internal node we calculate the maximum relative error in the Beltrami equations (9), i.e.,

$$\left|\frac{b(\eta)\,y_\eta}{Ma(\xi)\,x_\xi}-1\right|,\qquad \left|\frac{Ma(\xi)\,y_\xi}{b(\eta)\,x_\eta}+1\right|. \tag{35}$$

The partial derivatives are evaluated by a five-point, fourth-order accurate finite-difference formula. It might seem appropriate to use the Beltrami error as a convergence criterion rather than the boundary point displacements. However, we have found that, when the individual terms of the maximum Beltrami error are small (of order 10^{-3} with the present single-precision calculations), the round-off error may lead to a high Beltrami error even though the angles may be quite close to 90°. In addition to the Beltrami error, we calculate, for each node, the angle θ between the coordinate lines

$$\theta=\arccos\left(\frac{g_{12}}{h_\xi h_\eta}\right).$$

We have found that the maximum deviation from 90°, θ_M, did not necessarily occur at the node with the greatest Beltrami error, although it usually was found at a node in its neighborhood.

In most of the examples that follow, the boundaries are prescribed analytically so that the boundary functions F and their derivatives appearing in the Newton–Raphson solution of (29) and (30) could be calculated exactly. However, as this is often a tedious task, we use for all cases a cubic-spline representation of the boundaries.

Figure 4 is a test of the technique proposed for the case of the region defined by $z=\zeta^2$ with $\zeta=\xi+i\eta$ and $0\leqslant\xi,\eta\leqslant 1$. Here, the midpoint of the base corresponds to $\xi=0$, $\eta=0$ and is therefore a corner of the quadrilateral of aperture π. Since the mapping is required to be orthogonal, any corner at which the angle fails to be $\pi/2$ introduces a singularity. This circumstance is well known in the theory of conformal mapping and will be encountered in several other examples later on. However the mapping continues to be quasi-conformal, as the ratio of the stretchings introduced at this point is finite. For this region, the conformal module is

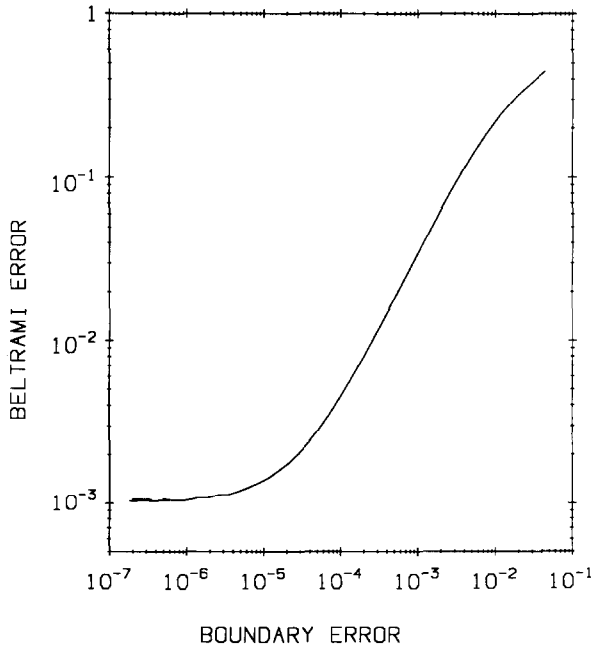

FIG. 5. Maximum Beltrami error versus maximum boundary error for the case of Fig. 4a. The iteration number is a parameter along the curve starting from the upper right and increasing toward the lower left. The flattening out of the lower left portion of the curve indicates a saturation of the Beltrami error due to round-off.

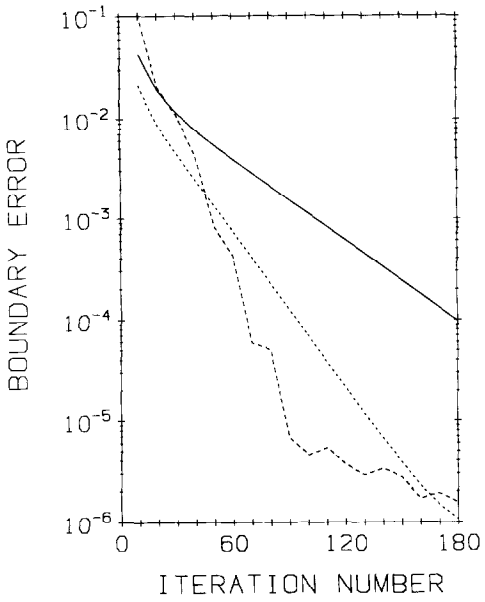

FIG. 6. Maximum boundary error versus iteration number for the calculation of Fig. 4a. The solid line corresponds to pure point-Newton–Raphson, the dotted line to over-relaxation on the boundary iterations only, and the dashed line to over-relaxation both on the boundary iteration and on the internal points. This result has been obtained by assuming an over-relaxation parameter equal to 1.9.

evidently unity. We first consider, in Fig. 4a, the conformal mapping for which $f = 1$. Here convergence required 179 iterations, the maximum error in the Beltrami equations was 0.4%, and the angle θ_M was 89.90°. The points where the maximum errors were found are close to the singular point.

To demonstrate the "saturation" of the Beltrami error as convergence is approached, in Fig. 5 we show a graph of the Beltrami error versus the boundary error for this calculation. The iteration number can be considered a parameter along this curve, increasing as one moves from the upper right toward the lower left. This progression is regular for most of the way toward convergence, but breaks down near the lower left part of the curve where round-off destroys the connection between the boundary and the Beltrami errors. Approach to convergence is shown in Fig. 6 in the form of the maximum boundary error versus iteration number. The solid line corresponds to pure point-Newton–Raphson, the dotted line has been obtained with overrelaxation on the boundary iterations, and the dashed line has been obtained with overrelaxation both on the boundary iteration and on the internal points. In this last calculation the overrelaxation correction was applied also to the computed position of the internal points as obtained from the solution of the field equations. The figure shows that a reduction in the number of iterations of a factor three is possible in this case for the same final error. This result has been obtained by assuming an overrelaxation parameter equal to 1.9, a choice that we have made no attempt to optimize.

Returning to the region of Fig. 4a, we demonstrate in Figs. 4b and c the degree of control achievable on the distribution of the coordinate lines by changing f. Figure 4b has been obtained with $f = p_1(\xi)/p_1(\eta)$, where $p_1(\xi) = 0.3k_1(0.1 + \xi^2)$. Here k_1 is a normalization constant required by the condition (15) and has the value $k_1 = 1000^{1/2}$ arc tan$(10^{1/2})/3 \simeq 13.3292$. This case required 221 iterations, with a maximum Beltrami error of approximately 2.6% and an angle of 89.21°. Figure 4c is for

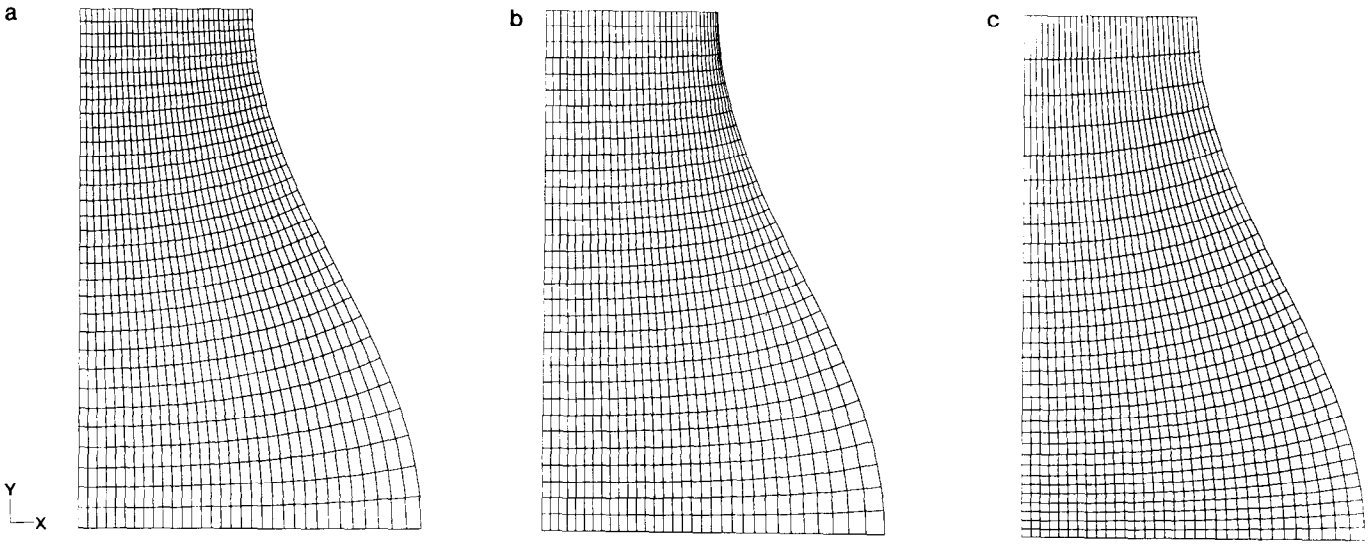

FIG. 7. The domain has three sides parallel to the x and y coordinate axes, while the fourth side is given by the equation $x = \frac{1}{2} + \frac{1}{6}\cos(\pi y)$, $0 \leqslant y \leqslant 1$. Figure 7a shows the mapping with $f = M$, while Figs. 7b and c show the mappings obtained with the distortion functions given in the text. The conformal module M was determined using the algorithm of Section IV.

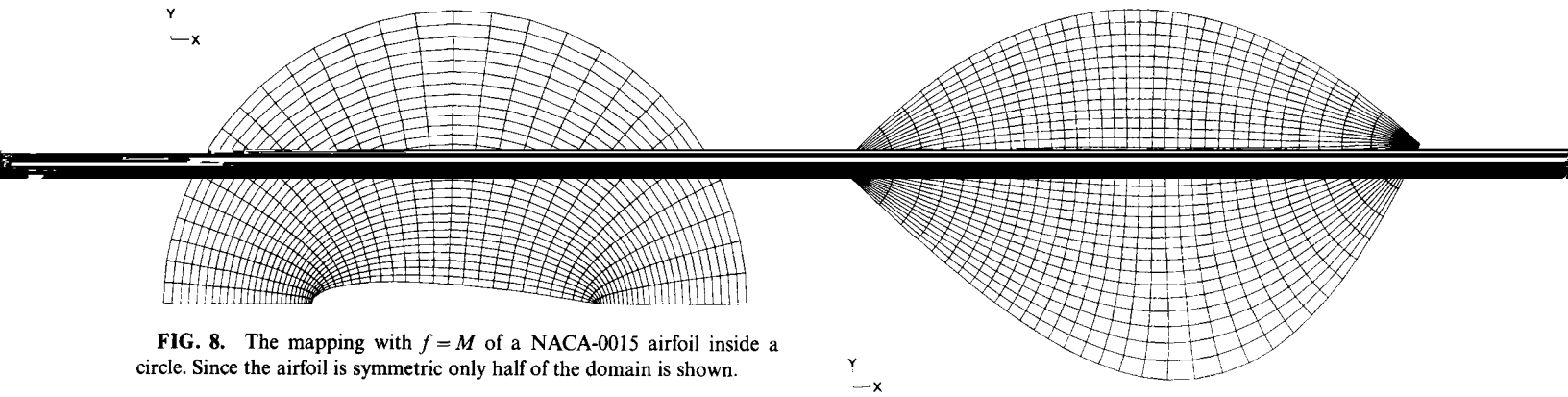

FIG. 8. The mapping with $f = M$ of a NACA-0015 airfoil inside a circle. Since the airfoil is symmetric only half of the domain is shown.

FIG. 10. Mapping of a lune with the two sides given by $y = x(1-x)$, and $y = -x(1-x^2)$, and f as in the text.

$f = p_2(\xi)$, with $p_2(\xi) = k_2(1 - 0.9\xi)$ and $k_2 = \frac{10}{9}\log 10 \simeq 2.5584$. This required 182 iterations with a maximum Beltrami error of 0.5% and an angle of 89.88°.

The region considered in the next series of examples in Figs. 7 is the same one of Ref. [18] for which the weak-constraint method of RL failed to converge. We have encountered no difficulties with our approach. Three sides are parallel to the coordinate axes and the fourth one is given by $x = \frac{1}{2} + \frac{1}{6}\cos(\pi y)$, $0 \leqslant y \leqslant 1$. The conformal module of this region, calculated by the method of Section IV, is found to have the value $M = 2.169603$. The mapping shown in Fig. 7a has been obtained by taking $f = M$. The maximum Beltrami error was 5.2%, and the angle $\theta_M = 89.71°$. For Fig. 7b, $f = Mp_1(\xi)/p_1(\eta)$, with p_1 as before. Here the Beltrami error was large, 80%, but the angle θ_M was quite satisfactory, 89.78°. In this example the maximum error occurs in the neighborhood of the upper right-hand corner, where the magnitude of the terms dividing in Eqs. (35) is small. This circumstance arises because the coordinate lines in that neighborhood are very nearly horizontal and vertical, which causes one of the Beltrami equations to become close to the trivial identity $0 = 0$. Use of double-precision arithmetic would presumably reduce this error which, however, appears to be of little significance. The last case for this region, shown in Fig. 7c, has been obtained with $f = M/p_2(\eta)$, with p_2 as before. Here the Beltrami error was 2%, and the angle 89.71°. These three cases required 221, 122, and 125 iterations, respectively.

Another set of examples is shown in Figs. 8 and 9. Figure 8 is the mapping for a NACA-0015 airfoil in a circle, obtained with $f = Mp_3(\xi)/p_3(\eta)$, with $M = 2.303574$, $p_3 = k_3(1 + 3\xi)$, and $k_3 = \frac{1}{3}\log 4 \simeq 0.4620981$. Since this airfoil is

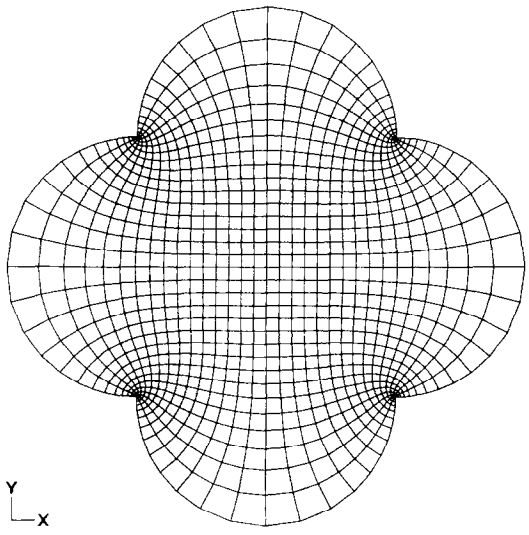

FIG. 9. Mapping with $f = M = 1$ of the domain obtained by constructing semi-circles on the four sides of the unit square.

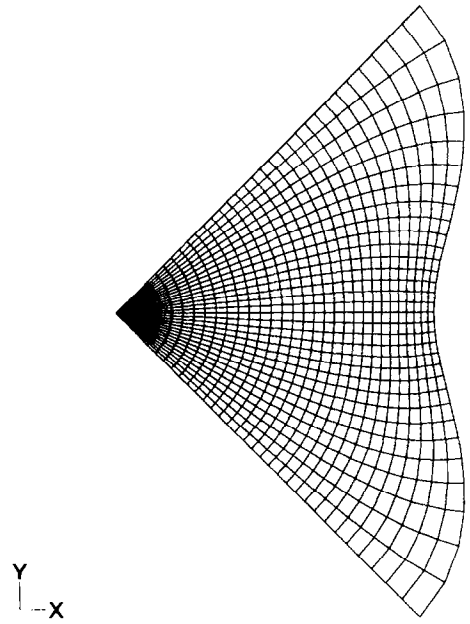

FIG. 11. Mapping of a trilateral with sides, $y = -x$, $y = x$, and $y = r(\theta)\sin(\theta)$ $x = r(\theta)\cos(\theta)$, with $r(\theta) = (1 - 0.2(2/\pi\theta)(1 - 2/\pi\theta))$, $\theta = \arctan(y/x)$, and f as in the text.

TABLE II

Details of the Computational Algorithm

Figure	M	Distortion function	θ_M	Beltrami error	Iterations
4a	1	M	89.90°	4.44×10^{-3}	179
4b	1	$Mp_1(\xi)/p_1(\eta)$	89.21°	2.64×10^{-2}	221
4c	1	$Mp_2(\xi)$	89.88°	5.58×10^{-3}	182
7a	2.169603	M	89.71°	5.15×10^{-2}	221
7b	2.169603	$Mp_1(\xi)/p_1(\eta)$	89.78°	8.0×10^{-1}	122
7c	2.169603	$M/p_2(\eta)$	89.71°	1.91×10^{-2}	125
8	2.303574	$Mp_3(\xi)/p_3(\eta)$	88.89°	6.20×10^{-1}	321
9	1	M	89.20°	5.26×10^{-3}	251
10	—	$\pi\xi(1-\xi)$	89.65°	—	205
11	—	$\pi\xi/2$	89.76°	—	156

Note. All calculations were performed in single precision with a boundary tolerance (see text) of 10^{-4}. The conformal module M for Figs. 4 and 9 is known exactly. The module for Figs. 7 and 8 is calculated using the algorithm described in Section IV. The regions in Figs. 10 and 11 are degenerate quadrilaterals with zero module. The quantity θ_M is the angle between the coordinate lines which exhibits the maximum deviation from 90°. $p_1(\xi) = 0.3k_1(0.1 + \xi^2)$, $p_2(\xi) = k_2(1 - 0.9\xi)$, $p_3(\xi) = k_3(1 + 3\xi)$, with $k_1 = 1000^{1/2}$ arc $\tan(10^{1/2})/3 \simeq 13.3292$, $k_2 = \frac{10}{9} \log 10 \simeq 2.558428$, $k_3 = \frac{1}{3} \log 4 \simeq 0.4620981$. These functions satisfy the restrictions detailed in Section III. For Figs. 10 and 11 the distortion function vanishes at the degenerate points (see text).

symmetric, only one-half of the domain is shown. This calculation required 321 iterations with a maximum Beltrami error of 68% and $\theta_M = 88.89°$, which is the maximum departure from orthogonality encountered in all examples. The geometry introduces a singularity at the trailing edge where the angle is not $\pi/2$. In Fig. 9, $f = M = 1$. The number of iterations was 251, the error 0.5%, and $\theta_M = 89.20°$.

Figures 10 and 11 are two examples of the mapping of degenerate quadrilaterals. Figure 10 is for a lune-shaped region the precise definition of which is given in the caption. In this case we have used for the distortion function the form (17) with $a = b = 1$. The quantity θ_M was 89.65° and 205 iterations were required. Figure 11 is for a trilateral of the special class considered in Section III and fully described in the caption. Here $f = \frac{1}{2}\pi\xi$ with $a = b = 1$. In this case 156 iterations were required and $\theta_M = 89.79°$. Since neither of these mappings is quasi-conformal, the Beltrami errors cannot be defined.

Several aspects of the numerical results described above are summarized in Table II.

VII. SUMMARY AND CONCLUSIONS

The orthogonal mapping technique proposed by Ryskin and Leal has been investigated, and several issues regarding its applicability have been clarified. An explicit class of distortion functions for the mapping equations, and suitable boundary conditions to be imposed on these equations, have been developed. The issue of the existence of the mapping for more general distortion functions (and the related issue of adaptivity) remain open questions, though a necessary condition that general distortion functions must satisfy has been obtained. The mapping method developed in this paper has been applied to problems for which the original method of RL fails.

A useful consequence of the factored form for the distortion function developed in Section III is that the mapping equations are separable and can therefore be efficiently solved by direct methods. In addition, partial differential equations, that were separable in the original Cartesian coordinate system, continue to be separable in the transformed coordinates. Since the computational domain is a square, advantage can be taken of this. For instance, rapid elliptic solvers developed for elliptic separable equations on rectangular domains [6] can be used for the solution of the transformed problem.

When compared with conformal mappings, the present method offers a much greater flexibility. It also appears to be quite stable in the sense that a slight alteration of the domain will not drastically change the mapping. Control of the distribution of the coordinate lines can be achieved through the proper selection of the functions a and b introduced in Section III. Further work on this aspect of the method is, however, necessary for the reasons indicated at the end of Section III.

Another useful aspect of the work described in this paper is a new technique for the computation of the conformal module of quadrilaterals. The examples shown seem to indicate that our approach has significant advantages over other available methods.

ACKNOWLEDGMENTS

Thanks are due to Dr. H. N. Oğuz for letting us use his boundary integral code. The public domain software library NETLIB [28] proved to be an invaluable source of reliable software. This study was supported by the N.S.F. under Grant MSM-8607732.

Note added in proof. Publication of this paper was greatly delayed by problems with the mail and other difficulties. Since the completion of this work we have successfully implemented a spectral version of the method which is currently used in a fluids code. These results will soon be ready for publication (H. N. Oğuz and A. Prosperetti, to be submitted to *J. Comp. Phys.*)

REFERENCES

1. J. F. Thompson, Z. U. A. Warsi, and C. W. Mastin, *J. Comput. Phys.* **47**, 1 (1982).
2. J. F. Thompson *et al.* Numerical Grid Generation: Foundations and Applications (North-Holland, New York, 1985).
3. P. R. Eiseman, *Ann. Rev. Fluid Mech.* **17**, 487 (1985).
4. C. W. Mastin, *Appl. Math. Comput.* **10**, 31 (1982).
5. S. A. Orszag, *J. Comput. Phys.* **37**, 70 (1980).

6. P. N. Swarztrauber, *SIAM J. Numer. Anal.* **11**, 1136 (1982).
7. P. Henrici, *Applied and Computational Complex Analysis, Vol. III* (Wiley, New York, 1986).
8. B. Fornberg, *SIAM J. Sci. Stat. Comput.* **1**, 386 (1980).
9. A. Seidl and H. Klose, *SIAM J. Sci. Stat. Comput.* **6**, 833 (1985).
10. G. T. Symm, *Numer. Math.* **9**, 250 (1966).
11. D. M. Hough and N. Papamichael, *Numer. Math.* **37**, 133 (1981).
12. G. Ryskin and L. G. Leal, *J. Comput. Phys.* **50**, 71 (1983).
13. R. Duraiswami, Ph.D. thesis, The Johns Hopkins University, Baltimore, 1990 (unpublished).
14. G. Ryskin and L. G. Leal, *J. Fluid Mech.* **148**, 1 (1983).
15. D. S. Dandy and L. G. Leal, *Phys. Fluids* **29**, 1360 (1986).
16. I. S. Kang and L. G. Leal, *Phys. Fluids* **30**, 1929 (1987).
17. E. P. Ascoli, D. S. Dandy, and L. G. Leal, *J. Comput. Phys.* **72**, 814 (1987).
19. L. V. Ahlfors, *Lectures on Quasiconformal Mappings* (Van Nostrand, Princeton, NJ, 1966).
20. O. Lehto and K. I. Virtaanen, *Quasiconformal Mappins in the Plane* (Springer-Verlag, Berlin, 1973).
21. Z. Nehari, *Conformal Mapping* (Dover, New York, 1975).
22. R. Arina, Orthogonal grids with adaptive control, in *Numerical Grid Generation in Computational Fluid Dynamics: Proceedings of the International Conference held at Landhust, West Germany, 1986*, edited by J. Hauser and C. Taylor (Pineridge Press, Swansea, UK, 1986), p. 113.
23. D. Gaier, *Lecture Notes in Mathematics, Vol. 399* (Springer-Verlag, Berlin, 1974).
24. D. Gaier, *Numer. Math.* **19**, 179 (1972).
25. L. N. Trefethen, *SIAM J. Sci. Stat. Comput.* **1**, 82 (1980).
26. L. N. Trefethen, *SCPACK* (version 2), Courant Institute of Mathematical Sciences, 1983 (unpublished).
27. J. Adams, P. Swarztrauber, and R. Sweet, *FISHPAK* (Version 3.1, October 1980) National Center For Atmospheric Research (unpublished).